Collision Preventing Phase-Progress Control for Velocity Adaptation in Human-Robot Collaboration

Dinmukhamed Zardykhan[1], Petr Svarny[2], Matej Hoffmann[2], Erfan Shahriari[1] and Sami Haddadin[1]

Abstract— **As robots are leaving dedicated areas on the factory floor and start to share workspaces with humans, safety of such collaboration becomes a major challenge. In this work, we propose new approaches to robot velocity modulation: while the robot is on a path prescribed by the task, it predicts possible collisions with the human and gradually slows down, proportionally to the danger of collision. Two principal approaches are developed—Impulse Orb and Prognosis Window—that dynamically determine the possible robot-induced collisions and apply a novel velocity modulating approach, in which the phase progress of the robot trajectory is modulated while the desired robot path remains intact. The methods guarantee that the robot will halt before contacting the human, but they are less conservative and more flexible than solutions using reduced speed and complete stop only, thereby increasing the effectiveness of human-robot collaboration. This approach is especially useful in constrained setups where the robot path is prescribed. Speed modulation is smooth and does not lead to abrupt motions, making the behavior of the robot also better understandable for the human counterpart. The two principal methods under different parameter settings are experimentally validated in a human-robot interaction scenario with the Franka Emika Panda robot, an external RGB-D camera, and human keypoint detection using OpenPose.**

Fig. 1: Human robot collaboration scenario where a human and a robot share the same workspace.

I. Introduction

With growing numbers of collaborative robots—industrial robots that work alongside or directly with humans in a shared space (see Fig. 1)—as well as personal/home robots, new solutions need to be developed to warrant safety and effectiveness of such collaboration. A fundamental demand in safe Human-Robot Interaction (HRI) is to prevent unintended robot-induced collisions, i.e. contacts where a moving robot part hits a human. This can be achieved through evasive movements of the robot (see I-A), but some tasks or setups (e.g., gluing, sawing) impose strict constraints on the robot end-effector path that do not allow such manoeuvres. Therefore, the only available action is to modify the task execution velocity, eventually halting if necessary.

We draw inspiration from the fact that humans are known to anthropomorphize their robot partners and prefer movements that have human-like characteristics [1], [2]. In particular, in handover tasks, people focus on the task space and modulate the velocity according to the cues from the partner [3]. Robot control with similar characteristics would thus be desired for two reasons: (i) Being closer to human expectations, it would be more predictable and perceived more natural; (ii) Smooth velocity modulation—as opposed to simple stopping—shortens the downtime of task execution.

[1]The authors are members of Munich School of Robotics and Machine Intelligence, Technical University of Munich, Munich, Germany, `firstname.lastname@tum.de`

[2]The authors are members of Department of Cybernetics, Czech Technical University in Prague, Czech Republic, `firstname.lastname@fel.cvut.cz`

In this work, we propose an approach whereby the robot always sticks to the prescribed path in the task space but modulates its speed relying on predictions of possible collisions with the human. This future-oriented component draws on the prediction of future positions of the robot, which are readily accessible.

A. State of the Art

Four modes of human-robot interaction can be distinguished [4], [5]: hand-guiding, safety-rated monitored stop, power and force limiting (PFL), and speed and separation monitoring (SSM). Hand-guiding does not allow autonomous operations of the robot and therefore is not suitable for our task. Safety-rated stop demands that the robot halts when the human enters the robot workspace and therefore this mode is not suitable for effective implementation of a highly collaborative task where the human often interferes with the robot workspace. PFL allows physical contact with a moving robot, but the impact force/pressure/energy need to be within specific limits, which constraints the mechanical characteristics of the robot (mass, shape, etc.) and its movement—speed in particular. The collision needs to be detected and responded to (see [6] for a survey). The limits can draw on preliminary versions of standards [5] employing the "pain threshold" methodology or on biomechanical injury data [7].

The last mode of collaboration is the Speed and Separation Monitoring regime, which demands that a protective separation distance is maintained at all times and that the robot stops before a collision can occur. This distance is derived from the relative speed of the robot and the human (or relying on worst-case values). The approaches, therefore, need to combine robust human detection and distance evaluation with fast robot control for efficient reaction (see [8] for a review of vision-based systems). Integrated devices are currently also being introduced for the detection of a human [9] or that support robot evasion and speed limiting [10].

Many of the approaches originate in the potential field approach [11] for obstacle avoidance. These obstacle-based repulsive fields were further developed into robot-based repulsive vectors or danger fields in the context of physical human-robot interaction [12], [13]. Repulsive vectors are also applied in humanoid robotics, for example, in connection with the so-called peripersonal space representations [14].

The necessary separation distances can be calculated dynamically from the properties of the system, e.g., velocities, stopping times, and distances [15], [16]. A related approach is the so-called kinetostatic danger field (KDF) [17], [18] that uses a precalculated safety field that is updated with the robot velocity and the human position to generate appropriate evasive action. So-called swept volumes based on a human kinematic model, i.e. prediction of space occupied by the human, allow the robot to generate evasive trajectories effectively [19].

B. Problem Statement and Contributions

In this work, we address the problem of safety in human-robot collaboration through smooth and predictive robot speed modulation, while keeping the planned end-effector path unchanged. More specifically, we design a novel collision prevention approach that smoothly modulates the rate of task progress according to anticipated collisions, which are detected based on the robot intended motions and the relative location of the human to the robot desired path. Two principal approaches are defined and experimentally validated under different parameter settings, including a combination of the two principal approaches.

This paper is structured as follows. The theory of the new methods is outlined in the next section. Section III briefly outlines the experimental setup and then results of experimental validation are presented and discussed. We close with discussion and future work.

II. Collision Preventing Phase-Progress Control

Considering $\boldsymbol{x} \in \mathbb{R}^3$ as the robot end-effector position, and $\boldsymbol{x}_d \in \mathbb{R}^3$ as the robot desired position, the objective is to prevent collision caused by the robot motion towards the human position at $\boldsymbol{x}_h \in \mathbb{R}^3$. The additional task constraint is that no deviation from the prescribed robot path is allowed. Therefore, a proposed solution to ensure collision prevention is to modulate the robot velocity. In the following section, first, we introduce a motion generation method that enables us to reduce the robot end-effector velocity while keeping the robot path intact. Afterwards, we present two collision preventing approaches to provide the amount of velocity reduction for the motion generator based on the collision possibility with respect to the robot intention.

A. Velocity Adaptation

The implementation of the above-mentioned methodology is as follows. The desired trajectory $\boldsymbol{x}_d$ is encoded as a function of a new variable $\phi \in [0,1]$ (i.e. $\boldsymbol{x}_d(\phi)$), where $\boldsymbol{x}_d(\phi=0)$ and $\boldsymbol{x}_d(\phi=1)$ correspond to the initial and final desired positions, respectively. Once the trajectory is defined one can progress through the phase by:

$$\phi = \int_0^t \Omega dt', \tag{1}$$

in which $\Omega \geq 0$ determines how fast the desired trajectory will reach the end. Now, in order to alter the speed, one can update Ω via:

$$\Omega^* = (1-\gamma)\Omega \tag{2}$$

where $\gamma \in [0,1]$, $\gamma \in \mathbb{R}$ is a braking variable that determines how much the robot should slow down (see Table I).

Braking value	The effect
$\gamma = 1$	Full stoppage
$0 < \gamma < 1$	Speed reduction
$\gamma = 0$	No speed reduction

TABLE I: The effect of the braking variable γ on the desired velocity.

The following two approaches will showcase how the braking variable γ is defined to achieve the collision prevention adaptation laws.

B. Approach I: Impulse Orb

Intuitively, in order to prevent a collision, the relative position $\boldsymbol{p}_h$ of the human with respect to the robot end-effector needs to be determined as follows:

$$\boldsymbol{p}_h = \boldsymbol{x}_h - \boldsymbol{x}. \tag{3}$$

Once the relative position is established, possible collisions can be anticipated from the relative distance $\|\boldsymbol{p}_h\|$, as well as from the robot intended motion. Naturally, if the robot intends to move in the direction of the human, the possibility of collision increases. The latter can be assessed by comparing the angle θ between the robot intended motion $\dot{\boldsymbol{x}}_d$ and the relative position $\boldsymbol{p}_h$ as shown in Fig. 2.

The behavior of the robot in the proximity of a human is defined by two spheres: a smaller one contained in a larger, both tangential to the end-effector (see Fig. 2). The space encapsulated by the outer sphere is called the Impulse Orb. The chance of collision when $\boldsymbol{x}_h$ is located within the smaller inner sphere is considered to be high, and when it is located outside the outer larger sphere, the chance is considered to be zero. Thus, the braking variable γ_{io} can be attributed to these two regions, as described in Table II.

Location of $\boldsymbol{x}_h$:	Braking value
Inside the inner sphere:	$\gamma_{io} = 1$
Outside the inner sphere and inside the outer sphere:	$0 < \gamma_{io} < 1$
Outside the outer sphere:	$\gamma_{io} = 0$

TABLE II: The braking variable γ_{io} based on the human location $\boldsymbol{x}_h$ with respect to the spheres of the Impulse Orb.

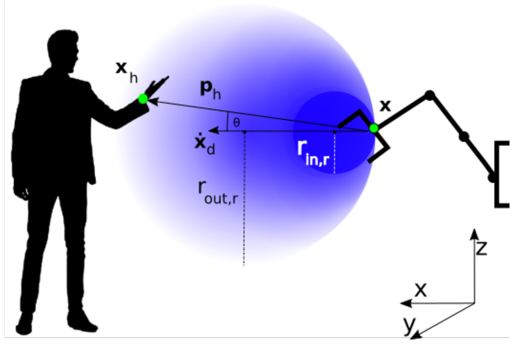

Fig. 2: A graphical representation of the Impulse Orb and the corresponding variables.

Considering $r_{\text{in},r}, r_{\text{out},r} \in \mathbb{R}^+$ as the radius of the inner and the outer spheres respectively, where $r_{\text{out},r} \geq r_{\text{in},r}$, the mathematical representation of the braking variable γ based on the location of human with respect to the Impulse Orb becomes

$$\gamma_{io} = \begin{cases} 1 & \text{if } \frac{0.5}{r_{\text{in,r}}} \leq \frac{\cos(\theta)}{\|\boldsymbol{p}_h\|} \\ \frac{1}{2}(1-\cos(\pi\frac{\frac{0.5\cos(\theta)}{\|\boldsymbol{p}_h\|}-\frac{1}{r_{\text{out},r}}}{\frac{1}{r_{\text{in},r}}-\frac{1}{r_{\text{out},r}}})) & \text{if } \frac{0.5}{r_{\text{out},r}} \leq \frac{\cos(\theta)}{\|\boldsymbol{p}_h\|} < \frac{0.5}{r_{\text{in},r}} \\ 0 & \text{else.} \end{cases} \tag{4}$$

In Fig. 3 as the human position $\boldsymbol{x}_h$ approaches from the outer sphere surface towards the inner sphere, the braking variable γ_{io} smoothly grows from 0 to 1 according to Eq. (4).

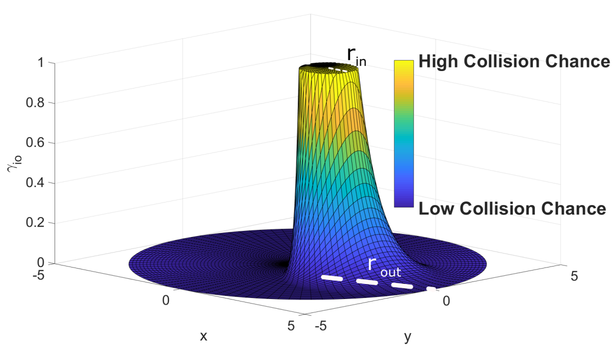

Fig. 3: The evolution of the braking variable γ_{io} over a planar cross section of an Impulse Orb with $r_{\text{in},r} = 0.075$ $[m]$ and $r_{\text{out},r} = 0.225$ $[m]$.

According to Eq. (4), the design of the Impulse Orb boils down to the choice of spheres' radii $r_{\text{in},r}$ and $r_{\text{out},r}$. To improve collision prevention, it makes sense to have larger radii for faster motions. On the other hand, having large radii for slower motions might lead to unnecessary braking. Thus, a reasonable design of the Impulse Orb would imply defining $r_{\text{in},r}$ and $r_{\text{out},r}$ as functions of the robot intended speed $\|\dot{\boldsymbol{x}}_d\|$ as follows:

$$r_{\text{in},r} = \kappa_{\text{in}}\|\dot{\boldsymbol{x}}_d\| \tag{5}$$

$$r_{\text{out},r} = \kappa_{\text{out}}\|\dot{\boldsymbol{x}}_d\| \tag{6}$$

where $\kappa_{\text{in}}, \kappa_{\text{out}} \in \mathbb{R}^+$ are the radius of the inner and outer spheres respectively, for $\|\dot{\boldsymbol{x}}_d\| = 1$ $[m/s]$.[1]

Substituting Eq. (5) and (6) into Eq. (4), the braking policy becomes[2]

$$\gamma_{io} = \begin{cases} 1 & \text{if } \frac{0.5}{\kappa_{\text{in}}} \leq \frac{\dot{\boldsymbol{x}}_d^T \boldsymbol{p}_h}{\|\boldsymbol{p}_h\|^2} \\ \frac{1}{2}(1-\cos(\pi\frac{\frac{0.5\dot{\boldsymbol{x}}_d^T\boldsymbol{p}_h}{\|\boldsymbol{p}_h\|^2}-\frac{1}{\kappa_{\text{out}}}}{\frac{1}{\kappa_{\text{in}}}-\frac{1}{\kappa_{\text{out}}}})) & \text{if } \frac{0.5}{\kappa_{\text{out}}} \leq \frac{\dot{\boldsymbol{x}}_d^T \boldsymbol{p}_h}{\|\boldsymbol{p}_h\|^2} < \frac{0.5}{\kappa_{\text{in}}} \\ 0 & \text{else.} \end{cases} \tag{7}$$

Hence, Eq. (7) defines a set for the braking variable γ based on the intended robot velocity, $\dot{\boldsymbol{x}}_d$), and the relative position of the human with respect to the robot end-effector ($\boldsymbol{p}_h$). Increasing the number of robot or human keypoints would not affect the proposed approach as it would essentially mean that there will be several relative vectors $\boldsymbol{p}_h$.

C. Approach II: Prognosis Window

In addition to instantaneous robot position and velocity w.r.t. human position (and possibly velocity), the planned robot path can be also exploited. An intuitive way to do so is to constantly consider a segment of the immediate upcoming robot desired path and inspect its relative distance to the human position. Hereinafter, this segment is called the *Prognosis Window*.

Considering $\boldsymbol{x}_d(\phi)$ as the robot desired position at the current phase, the length of the Prognosis Window can be determined by the amount of phase progression Δ, where $\Delta = \{\Delta \in \mathbb{R} | 0 \leq \Delta \leq 1\}$, such that $\boldsymbol{x}_d(\phi + \Delta)$ is the desired position at the end of the window. Throughout this window, $n \in \mathbb{N}$ regions can be set with the phase progression δ such that

$$\delta = \frac{\Delta}{n}. \tag{8}$$

The relative distance of the Prognosis Window to the human can be evaluated by determining the distance between the human position and the desired robot position at the edge of each of the aforementioned regions (i.e. $\boldsymbol{x}_d(\phi), \boldsymbol{x}_d(\phi + \delta), \ldots, \boldsymbol{x}_d(\phi + n\delta)$).

Depending on the task, the significance of human proximity to each of these regions might vary. This can be employed by associating different non-negative weights $\alpha_i, i \in \{0, \ldots, n\}$ to different regions. Thus a weighted proximity for each of the selected points inside the Prognosis Window can be defined as

$$\psi_i = \frac{\alpha_i}{\|\boldsymbol{x}_d(\phi + i\delta) - \boldsymbol{x}_h\|}, \qquad i \in \{0, 1, \ldots, n\}, \tag{9}$$

and the overall weighted proximity becomes

$$\psi = \sum_{i=0}^{n} \psi_i. \tag{10}$$

Two spheres that are centered at the human position are defined with the radii $r_{\text{in},h}, r_{\text{out},h} \in \mathbb{R}^+$ where $r_{\text{out},h} \geq r_{\text{in},h}$. When the whole Prognosis Window is outside the outer sphere, the situation is considered to be safe and there is no

[1] See Section III-D for a discussion of the possible values.

[2] Please note that $\dot{\boldsymbol{x}}_d^T \boldsymbol{p}_h = \|\dot{\boldsymbol{x}}_d\| \ \|\boldsymbol{p}_h\| \ \cos(\theta)$.

need for the robot to reduce speed. On the other hand, when the whole Prognosis Window is inside the inner sphere, a full stop is necessary. Thus, the braking variable γ_{pw} can be associated with these situations as described in Table III.

Location of the Prognosis Window:	Braking value
Inside the inner sphere:	$\gamma_{pw} = 1$
Outside the inner sphere and inside the outer sphere:	$0 < \gamma_{pw} < 1$
Outside the outer sphere:	$\gamma_{pw} = 0$

TABLE III: The braking variable γ_{pw} based on the relative location of the Prognosis Window w.r.t. the two virtual spheres around the human.

To verify the relative location of the Prognosis Window with the two spheres, the following boundaries for braking are defined

$$\psi_{\text{in}} = \sum_{i=0}^{n} \frac{\alpha_i}{r_{\text{in}}}, \tag{11}$$

$$\psi_{\text{out}} = \sum_{i=0}^{n} \frac{\alpha_i}{r_{\text{out}}}. \tag{12}$$

The braking policy then becomes

$$\gamma_{pw} = \begin{cases} 1 & \text{if } \psi \geq \psi_{\text{in}}, \\ \frac{1}{2}(1+\cos(\pi\frac{\psi_{\text{in}}-\psi}{\psi_{\text{in}}-\psi_{\text{out}}})) & \text{if } \psi_{\text{in}} > \psi \geq \psi_{\text{out}}, \\ 0 & \text{else,} \end{cases} \tag{13}$$

where the braking variable γ_{pw} smoothly grows from 0 to 1, when the Prognosis Window enters the outer sphere and approaches to the inner sphere.

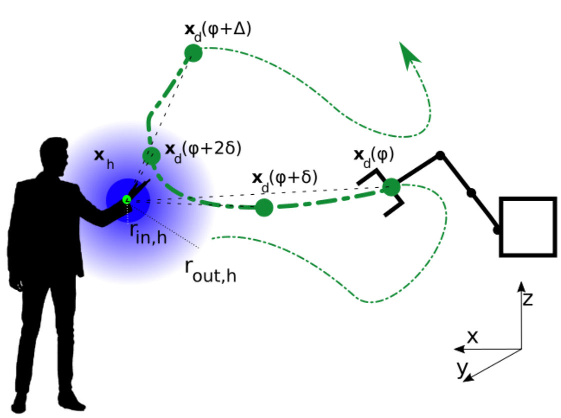

Fig. 4: A graphical represenation of the Prognosis Window and the corresponding variables.

D. Fused Approaches

Both Impulse Orb and Prognosis Window approaches prevent robot-induced collisions. Based on previously conducted experiments, the Impulse Orb approach has shown to be the most effective in more dynamic environments. On the other hand, Prognosis Window has shown effectiveness in rather static situations. As the real world contains an unpredictable blend of both these situations, we suggest combining both approaches for effectiveness and versatility. Depending on a situation when one method would be preferred while maintaining the benefits of the other, a prioritization strategy can be introduced. Subsequently, the final velocity adaptation law from Eq. (2) becomes

$$\Omega^* = (1 - \frac{\beta_{io}\gamma_{io} + \beta_{pw}\gamma_{pw}}{\beta_{io} + \beta_{pw}})\Omega, \tag{14}$$

where β_{io} and β_{pw} are non-negative priority weights that determine the efficacy of each braking policy. Obviously, assigning zero priority to either approach nullifies its effect on the overall adaptation of the velocity. The overall velocity adaptation approach is depicted in Fig. 5.

The proposed approach essentially scales down the velocity. This can be viewed as a damping effect. Considering that the original desired trajectory complies with the overall stability of the system, the proposed approach would not violate stability. Moreover, as mentioned previously, it is always assumed that the system is able to follow the introduced modulation on the desired velocity and the possible constraints would not jeopardize this; similar assumptions were in [20].

III. EXPERIMENTAL VALIDATION

In this section, the proposed approaches are implemented, tested, and the effect of the corresponding variables is demonstrated. The 7DoF Franka Emika Panda robot with a properly tuned Cartesian Impedance controller is used to perform a point-to-point motion, while a human, one of the authors, is present within the manipulator workspace (see Fig. 1). The Intel RealSense®D435 RGB-D camera is used as a vision unit to locate the human. The calibration was performed with respect to the robot base with the use of ArUco markers. The camera resolution is 848×480, and its default settings are used. The image is processed by the camera's Python API (2.17.1) [21] and OpenCV3 [22]. Colour images are processed by the OpenPose library [23] that calculates the estimated human keypoints based on the BODY-25 model. The keypoint locations found are deprojected using the aligned depth image. For the sake of clarity, only the end-effector and human wrist keypoints are taken into consideration. The latter are OpenPose's keypoints 4, 7 (see Fig. 6). Experiments with more keypoints are planned to be included in future work.

All the experiment types along with visualization of the important features (Impulse Orb / Prognosis Window) are illustrated in the accompanying video.

A. Experiment I: Impulse Orb

To test the Impulse Orb approach, a linear, phase-based, point-to-point motion is set as the desired end-effector trajectory. The end-effector moves with the maximal velocity 0.3 $[m/s]$ and in total covers 1 $[m]$ length on the x-axis. The human wrist is at 0.35 $[m]$ on the x-axis and 0.12 $[m]$ on the y-axis (see Fig. 7 and Fig. 8). The Impulse Orb is designed with $r_{\text{in},r}$ and $r_{\text{out},r}$ respectively set to 0.15 $[m]$ and 0.45 $[m]$.

To verify the effectiveness of the Impulse Orb approach, it is compared with another SSM approach: the Reduced

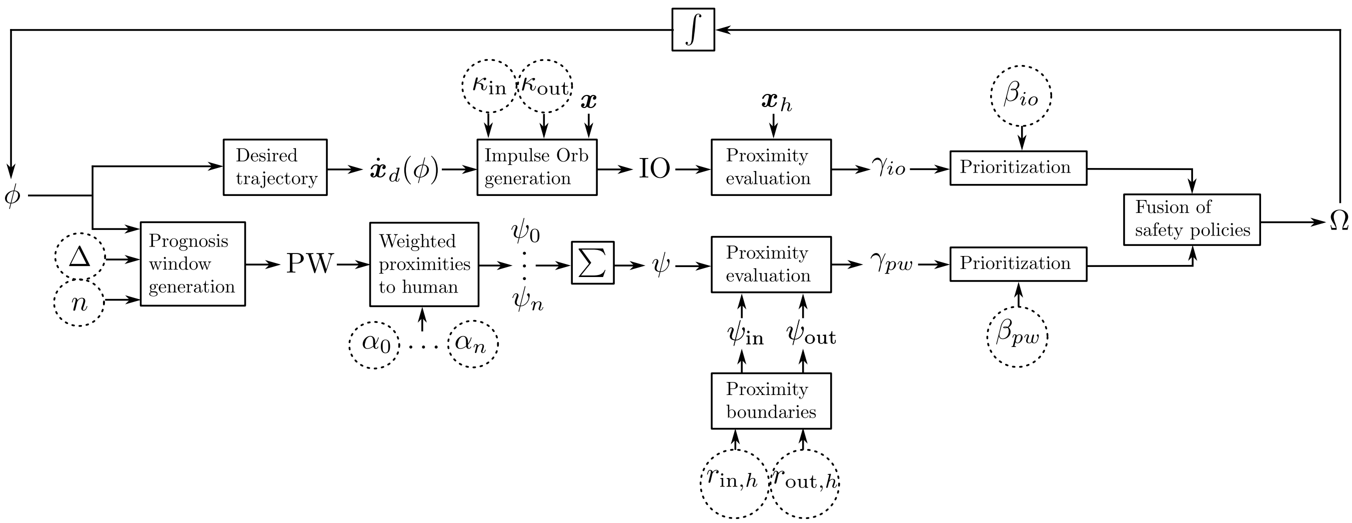

Fig. 5: Block diagram of the overall safety-ensuring velocity adaptation law. The tunable parameters are indicated in circles.

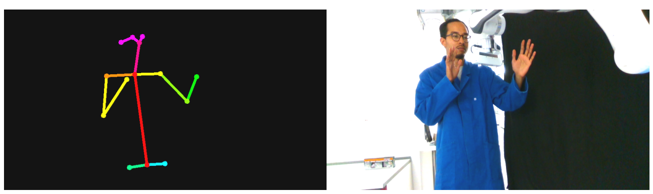

Fig. 6: Openpose detected keypoints and camera view.

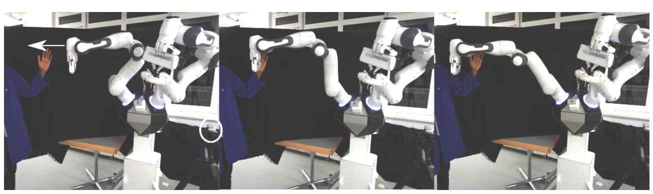

Fig. 7: Impulse Orb Experiment I: a collision prediction zone is constantly verifying the possible collisions based on the instantaneous robot motion and the human position detected by the camera.

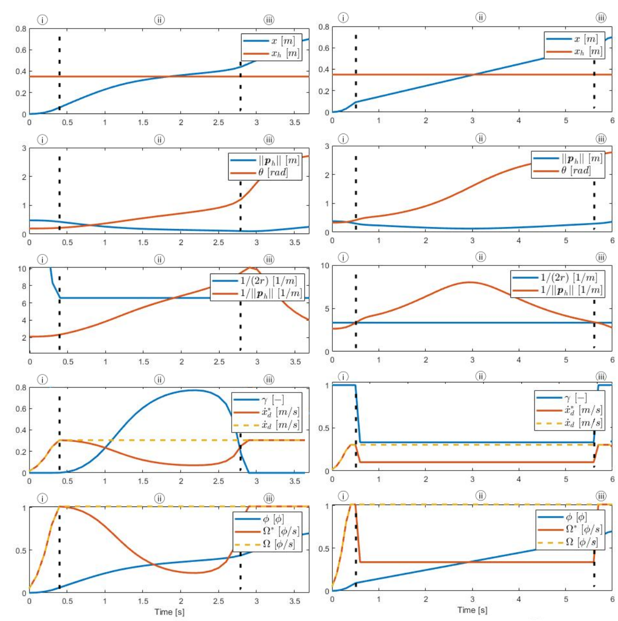

Fig. 8: Impulse Orb (left), Reduced Speed Zone (right).

Speed Zone [5], [24] where a fixed-sized sphere with the radius of 0.3 $[m]$ is defined around the robot end-effector such that when the human is detected inside the sphere, the desired speed is reduced to $1/3$ of the original speed. As can be seen in Fig. 8 in segment i, when the desired velocity grows, the Impulse Orb size also grows. This can be seen through the reduction of $1/(2r_{\text{in},r})$ and $1/(2r_{\text{out},r})$. The size of the Reduced Speed Zone remains the same.

In the segment ii in the Impulse Orb approach, it is visible that when the end-effector position $\boldsymbol{x}$ approaches the hand position $\boldsymbol{x}_h$ (i.e. where $\|\boldsymbol{p}_h\|$ is adequately reduced), the relative angle θ starts to grow. This signifies that the hand enters the Impulse Orb, and thus, the braking variable γ_{io} starts to have non-zero values. Therefore, the shaped desired velocity $\dot{\boldsymbol{x}}_d$ smoothly decreases via the reduced Ω^*. As soon as the end-effector passes the hand along the x-axis, the braking variable γ_{io} changes to zero and the shaped desired velocity $\dot{\boldsymbol{x}}_d^*$ becomes the same value as the original $\dot{\boldsymbol{x}}_d$ because the wrist is outside the Impulse Orb region. This can be seen especially in the experiment segment iii.

In contrast to the explained behavior, when using the Reduced Speed Zone, in segment ii, the shaped desired velocity $\dot{\boldsymbol{x}}_d^*$ is suddenly reduced to the $1/3$ of the original velocity $\dot{\boldsymbol{x}}_d$. This effect continues even when the robot end-effector passes the hand position in the x-direction, which is not an unsafe situation anymore. Thus, in the safe segment, iii the robot is still forced to move at a slow pace unnecessarily.

Exp.	Δ	n	α_0	α_1	α_2	α_3	$r_{\text{in},h}$	$r_{\text{out},h}$
II-A	0.045	3	4	3	2	1	0.05 $[m]$	0.15 $[m]$
II-B	0.045	3	1	2	3	4	0.05 $[m]$	0.15 $[m]$
II-C	0.45	3	4	3	2	1	0.05 $[m]$	0.15 $[m]$

TABLE IV: Parametetrization for the Prognosis Window experiments.

Exp.	β_{io}	β_{pw}
III-A	1	0
III-B	0	1
III-C	0.5	0.5

TABLE V: The prioritization of the approaches during the fusion.

B. Experiment II: Prognosis Window

These experiments investigate the Prognosis Window approach and the effect of the choices of the window length Δ and the proximity weights α_i as explained in Section II-C. There are three conducted experiments with different parametrization, as shown in Table IV.

In all three experiments, the desired end-effector trajectory is encoded to a cyclic motion along the x-axis. Considering the phase (Eq. (1)) and the velocity adaption law (Eq. (2)):

$$x_d = 0.35\cos(2\pi\phi) - 0.35, \tag{15}$$

$$\dot{x}_d = -0.7\pi\Omega^* \sin(2\pi\phi), \tag{16}$$

and the phase progression pace is originally set to $\Omega = 0.1\ [\phi/s]$. The human hand is located along the x-axis of the desired path $0.04\ [m]$ (see Fig. 9).

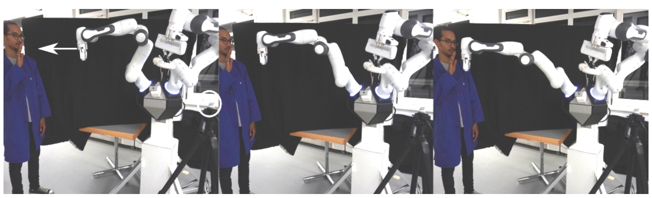

Fig. 9: Prognosis Window Experiment II: robot is able to predict possible collisions in the upcoming phases, with the help of camera indicated by circle.

As can be seen in Fig. 10, segment a, because the length of the Prognosis Window for the Experiments II-A and II-B is short, it takes longer for the window to enter into the outer sphere around the human hand. This is different from the Experiment II-C where the window size is 10 times longer.

On the other hand, when the Prognosis Window enters into the outer sphere, and the braking variable γ_{pw} starts to grow, the long length of the window in Experiment II-C allows for the prediction to foresee the return path, leading to the conclusion that no collision would occur. Thus, although for the experiment II-C the braking variable grows during segment b, it never becomes 1 as opposed to the Experiments II-A and II-B. As a result, the robot desired motion stops during the Experiments II-A and II-B, and it does not stop in the Experiment II-C.

Moreover, the effect of proximity weight distribution α_i on the braking behavior can be seen in the differences between Experiments II-A and II-B. The coefficient weights are distributed more towards the future (i.e. $\alpha_{i+1} > \alpha_i$) in the Experiment II-B, so the robot detects the danger faster. As a result, it stops $0.02\ [m]$ earlier than in the Experiment II-A for which the weights are distributed more towards the current phase (i.e. $\alpha_{i+1} < \alpha_i$). This effect is more visible when the length of the Prognosis Window is large enough so that the variance of the desired position over the window is adequately high.

C. Experiment III: Fused Safety Approaches

As explained in Section II-D, both approaches should warrant that the robot stops prior to collision and they were experimentally validated to be safe. Although both of them were performing better than the Reduced Speed Zone approach, in certain situations, they were over-conservative ("false positive speed reductions"), suggesting that the performance on the task can still be improved.

The fusion of these approaches via Eq. 14 increases the effectiveness as demonstrated in the following series of experiments. The robot is supposed to follow the same motion as in Eq. 15, 16. However, this time, both human hands are in the collaborative workspace and interfere with the robot movement. The left hand is located at $0.35\ [m]$ on the x-axis and $0.05\ [m]$ on the y-axis, and the right hand is located $0.05\ [m]$ far from the end of the desired path (see Fig. 11). The applied human detection considers the closest hand to the end-effector for the safety evaluation and the same parameters are used for each of the approaches as were in the previous experiments; the prioritization parameters β are set according to Table V.

As seen in Fig. 12, the system becomes over-conservative when only the Impulse Orb approach is being used. The robot approaches the edge of the motion and because it assumes that a collision is going to occur, the associated γ increases and as a result the robot will stop. On the other hand, as seen in Fig. 13 when only the Prognosis Window is being used and the size of windows is not being well-tuned, the end-effector can undergo a premature stoppage even though the trajectory is not directed towards the human position but only in the vicinity of a human. As a result, also in this case, the robot would stop. Although in both cases no collision would occur the effectiveness of the overall behavior can grow by fusing both approaches in Experiment III-C. Here, the robot does not stop and still, no collision would occur.

D. Discussion

The Impulse Orb, the Prognosis Window, and the combination of both approaches were tested in a real-time application. The following points should be noted:

First of all, the robot must be capable of tracking the desired motions for the velocity adaptation to take effect.

Secondly, different criteria can be used for the parametrization of the approaches. For instance, the size of the Impulse Orb (i.e.$r_{\text{in},r}$ and $r_{\text{out},r}$) could be adapted by using the reflected mass, as suggested in [7]. Alternatively, the length of the Prognosis Window, Δ, can also be adapted such that the amount of the future-prognosis is adequate for the task at hand. Also, the choice of variable n can depend

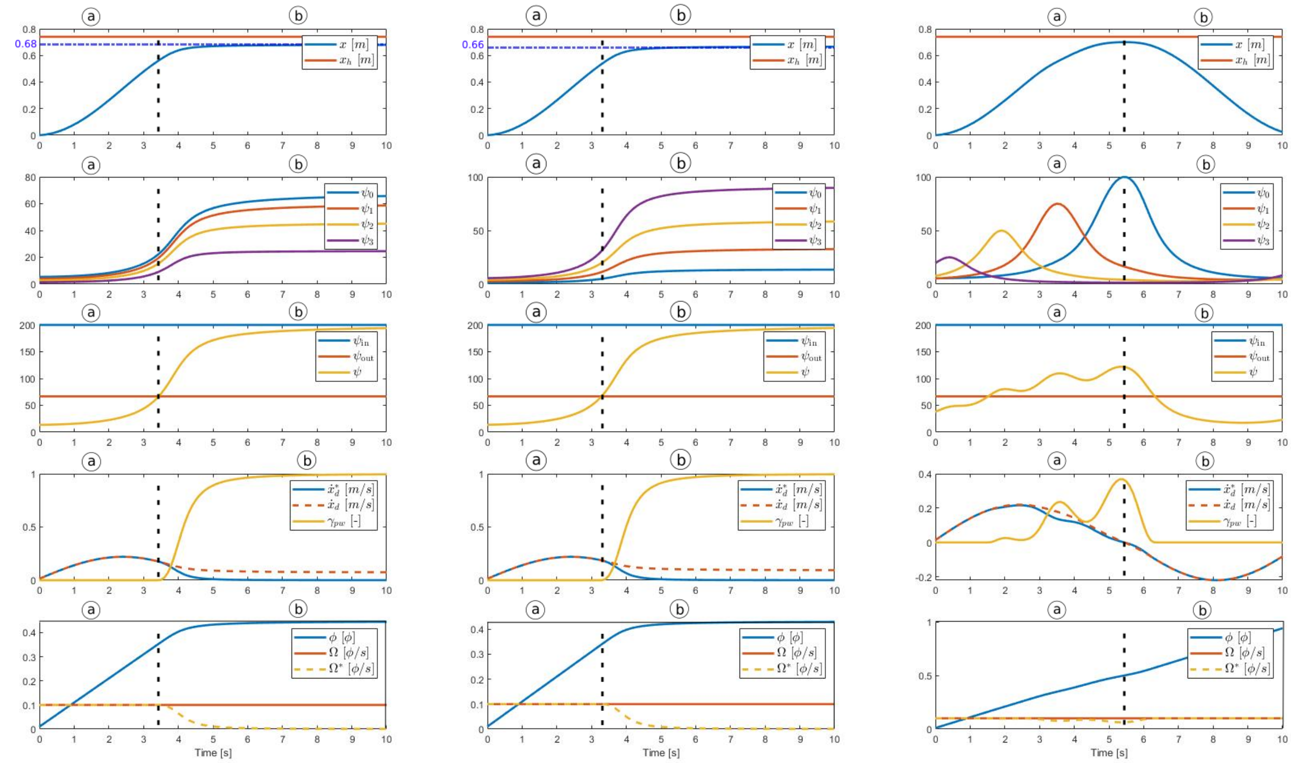

Fig. 10: Experiment for the Prognosis Window approach. From left to right the Exp. II-A and Exp. II-B for short window and Exp. II-C on right for long window.

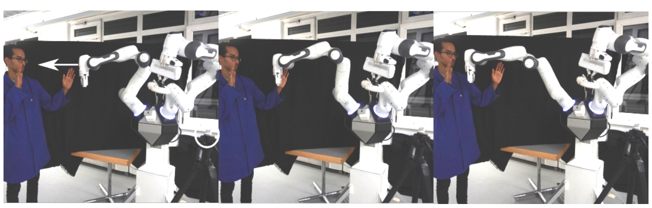

Fig. 11: Experiment III - Setup with indicated camera and robot end-effector movement.

on path variance. For instance, for a highly varying path, a bigger n is preferred to provide an adequate estimation of upcoming collisions.

It should be noted that our current approach did not follow any specific velocity dampening strategy neither did it slow down to a specific velocity value that would be considered as safe (either by standards or data-driven approaches [7]). This can be part of future work.

Last, human detection does not need to be a keypoint-based detection, as in the presented case. However, the keypoint-based approach allows a higher resolution of the human position than classical approaches and thereby allows the robot to react only when necessary. Similarly, the resolution of the robot position could be improved by considering the whole robot and not only the end-effector. This extension would be especially desirable in the case of humanoid robots as they might collide with humans in multiple ways.

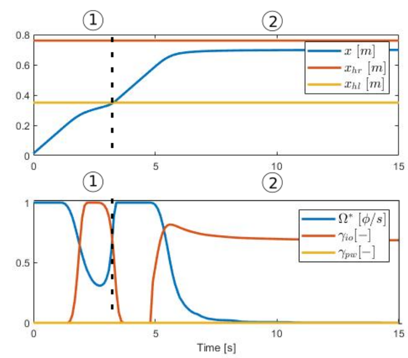

Fig. 12: Exp. III-A - Only Impulse Orb prioritized.

However, the current method is already directly applicable to a dual-arm setup.

IV. Conclusion and Future Work

We presented two methods to smoothly modulate robot velocity taking into account the presence of human operator as well as the instantaneous and intended robot trajectory: (i) the Impulse Orb approach is based on immediate proximity in the end-effector movement direction; (ii) the Prognosis Window approach takes into account a future segment of the end-effector trajectory. When applied individually, both methods were found to be still overly conservative, i.e. reducing the robot speed more than necessary. Best results

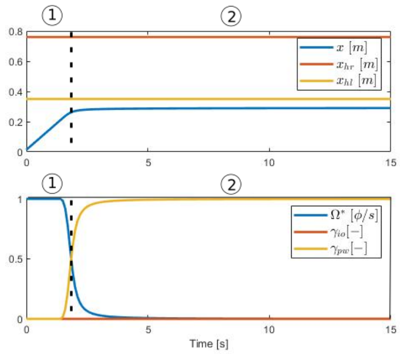

Fig. 13: Exp. III-B - Only Prognosis Window prioritized.

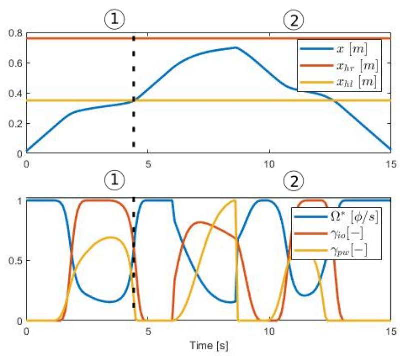

Fig. 14: Exp. III-C - Fusion of both methods with equal priorities.

were achieved with their combination, which constitutes a versatile tool for safe, effective and human-friendly speed modulation of the robot. We verified the suggested methods in an interactive setup with a Franka Emika Panda robot platform, with human keypoints detected using an external RGB-D camera and feeding the OpenPose network.

V. ACKNOWLEDGMENTS AND CONFLICTS

We gratefully acknowledge the funding of this work by the BMBF IKT 2020 MobIPaR project (No. V4IIP003), European Unions Horizon 2020 research and innovation programme project ILIAD (No. 732737) and Alfried Krupp von Bohlen und Halbach Foundation.

P.S. and M.H. were supported in part by the European Regional Development Fund under project "Research Center for Informatics" (CZ.02.1.01/0.0/0.0/16_019/0000765) and Czech Science Foundation under Project GA17-15697Y. P.S. was also partially supported by the Czech Technical University in Prague, grant No. SGS18/138/OHK3/2T/13.

Please note that S. Haddadin has a potential conflict of interest as shareholder of Franka Emika GmbH.

REFERENCES

[1] A. Kupferberg, S. Glasauer, M. Huber, M. Rickert, A. Knoll, and T. Brandt, "Biological movement increases acceptance of humanoid robots as human partners in motor interaction," *AI & society*, vol. 26, no. 4, pp. 339–345, 2011.

[2] B. Mutlu, A. Terrell, and C.-M. Huang, "Coordination mechanisms in human-robot collaboration," in *Proceedings of the Workshop on Collaborative Manipulation, 8th ACM/IEEE International Conference on Human-Robot Interaction*, pp. 1–6, Citeseer, 2013.

[3] A. Moon, D. M. Troniak, B. Gleeson, M. K. Pan, M. Zheng, B. A. Blumer, K. MacLean, and E. A. Croft, "Meet me where i'm gazing: how shared attention gaze affects human-robot handover timing," in *Proceedings of the 2014 ACM/IEEE international conference on Human-robot interaction*, pp. 334–341, ACM, 2014.

[4] "ISO 10218 Robots and robotic devices – Safety requirements for industrial robots," standard, International Organization for Standardization, Geneva, CH, 2011.

[5] "ISO/TS 15066 Robots and robotic devices – Collaborative robots," standard, International Organization for Standardization, Geneva, CH, 2016.

[6] S. Haddadin, A. De Luca, and A. Albu-Schäffer, "Robot collisions: A survey on detection, isolation, and identification," *IEEE Transactions on Robotics*, vol. 33, no. 6, pp. 1292–1312, 2017.

[7] N. Mansfeld, M. Hamad, M. Becker, A. G. Marin, and S. Haddadin, "Safety map: A unified representation for biomechanics impact data and robot instantaneous dynamic properties," *IEEE Robotics and Automation Letters*, vol. 3, no. 3, pp. 1880–1887, 2018.

[8] R.-J. Halme, M. Lanz, J. Kämäräinen, R. Pieters, J. Latokartano, and A. Hietanen, "Review of vision-based safety systems for human-robot collaboration," *Procedia CIRP*, vol. 72, no. 1, pp. 111–116, 2018.

[9] A. M. Zanchettin, P. Rocco, S. Chiappa, and R. Rossi, "Towards an optimal avoidance strategy for collaborative robots," *Robotics and Computer-Integrated Manufacturing*, vol. 59, pp. 47–55, 2019.

[10] S. Murray, W. Floyd-Jones, Y. Qi, D. J. Sorin, and G. Konidaris, "Robot motion planning on a chip.," in *Robotics: Science and Systems*, 2016.

[11] O. Khatib, "Real-time obstacle avoidance for manipulators and mobile robots," in *Autonomous robot vehicles*, pp. 396–404, Springer, 1986.

[12] F. Flacco, T. Kroeger, A. De Luca, and O. Khatib, "A depth space approach for evaluating distance to objects," *Journal of Intelligent & Robotic Systems*, vol. 80, no. 1, pp. 7–22, 2015.

[13] B. Lacevic, P. Rocco, and A. M. Zanchettin, "Safety assessment and control of robotic manipulators using danger field," *IEEE Transactions on Robotics*, vol. 29, no. 5, pp. 1257–1270, 2013.

[14] D. H. P. Nguyen, M. Hoffmann, A. Roncone, U. Pattacini, and G. Metta, "Compact real-time avoidance on a humanoid robot for human-robot interaction," in *Proceedings of the 2018 ACM/IEEE International Conference on Human-Robot Interaction*, pp. 416–424, ACM, 2018.

[15] F. Vicentini, N. Pedrocchi, M. Giussani, and L. M. Tosatti, "Dynamic safety in collaborative robot workspaces through a network of devices fulfilling functional safety requirements," in *ISR/Robotik 2014; 41st International Symposium on Robotics*, pp. 1–7, VDE, 2014.

[16] C. Byner, B. Matthias, and H. Ding, "Dynamic speed and separation monitoring for collaborative robot applications–concepts and performance," *Robotics and Computer-Integrated Manufacturing*, vol. 58, pp. 239–252, 2019.

[17] M. P. Polverini, A. M. Zanchettin, and P. Rocco, "A computationally efficient safety assessment for collaborative robotics applications," *Robotics and Computer-Integrated Manufacturing*, vol. 46, pp. 25–37, 2017.

[18] B. Lacevic and P. Rocco, "Kinetostatic danger field-a novel safety assessment for human-robot interaction," in *2010 IEEE/RSJ International Conference on Intelligent Robots and Systems*, pp. 2169–2174, IEEE, 2010.

[19] M. Ragaglia, A. M. Zanchettin, and P. Rocco, "Trajectory generation algorithm for safe human-robot collaboration based on multiple depth sensor measurements," *Mechatronics*, vol. 55, pp. 267–281, 2018.

[20] S. Haddadin, A. Albu-Schaffer, A. De Luca, and G. Hirzinger, "Collision detection and reaction: A contribution to safe physical human-robot interaction," in *2008 IEEE/RSJ International Conference on Intelligent Robots and Systems*, pp. 3356–3363, IEEE, 2008.

[21] Intel, "librealsense." `https://github.com/IntelRealSense/librealsense`, 2018. Version 2.17.1; Accessed: 2019-02-24.

[22] G. Bradski, "The OpenCV Library," *Dr. Dobb's Journal of Software Tools*, 2000.

[23] Z. Cao, G. Hidalgo, T. Simon, S.-E. Wei, and Y. Sheikh, "OpenPose: realtime multi-person 2D pose estimation using Part Affinity Fields," in *arXiv preprint arXiv:1812.08008*, 2018.

[24] A. Albu-Schäffer, C. Ott, and G. Hirzinger, "A unified passivity-based control framework for position, torque and impedance control of flexible joint robots," *The international journal of robotics research*, vol. 26, no. 1, pp. 23–39, 2007.